Progress in Natural Science: Materials International 28 (2018) 194–199

HOSTED BY

Contents lists available at ScienceDirect

Progress in Natural Science: Materials International

journal homepage: www.elsevier.com/locate/pnsmi

Original research

Dehydrogenation and reaction pathway of Perovskite-Type $NH_4Ca(BH_4)_3$

Chengguang Lang[a,c], Yi Jia[b,c,*], Jiangwen Liu[a], Hui Wang[a], Liuzhang Ouyang[a,c,*], Min Zhu[a,c], Xiangdong Yao[b,c]

[a] School of Materials Science and Engineering, Guangdong Provincial Key Laboratory of Advanced Energy Storage Materials, South China University of Technology, Guangzhou 510641, China
[b] School of Natural Sciences and Queensland Micro, and Nanotechnology Centre, Griffith University, Nathan, QLD 4111, Australia
[c] China-Australia Joint Laboratory for Energy & Environmental Materials, Joint Venture of Griffith University and South China University of Technology, Nathan, QLD 4111, Australia

ARTICLE INFO

Keywords:
Metal borohydride
Perovskite
$NH_4Ca(BH_4)_3$
Hydrogen storage materials
Solid-state NMR

ABSTRACT

Perovskite-type borohydride, $NH_4Ca(BH_4)_3$, is considered as a promising hydrogen storage material due to its high gravimetric hydrogen capacity (15.7 wt%). In this work, the dehydrogenation performance and reaction pathway of $NH_4Ca(BH_4)_3$ have been systematically investigated. It is found that the initial decomposition temperature is only 65 °C, suggesting a low thermodynamic stability of $NH_4Ca(BH_4)_3$. The desorption kinetics conducted by differential scanning calorimetry (DSC) indicates that the activation energy of decomposition is about 226.1 kJ/mol. The dehydrogenation pathway of $NH_4Ca(BH_4)_3$ characterized by fourier-transform infrared spectroscopy (FTIR) and solid-state nuclear magnetic resonance (NMR) shows a stepwise decomposition process, in which the initial dehydrogenation is due to destabilization of H^+ in NH_4 and H^- in BH_4 followed by the subsequent dehydrogenation steps arising from the decomposition of homologous NH_3BH_3 and the final decomposition of $Ca(BH_4)_2$ at a high temperature, respectively.

1. Introduction

Metal borohydrides $M(BH_4)_n$ (M = Li, Na, K, Mg, Ca, etc.) have tremendous potential in the realm of clean fuels due to their low molecular weight and high hydrogen storage capacity. For example, $LiBH_4$ as a solid state hydrogen storage material can release 13.8 wt% of hydrogen according to the dehydriding reaction as below [1–4]:

$$LiBH_4 \rightarrow LiH + B + 3/2H_2 \quad (1)$$

However, the metal borohydrides need high temperature to release hydrogen owing to their high thermal stability and slow kinetics. The first-principles calculations reveal that the charge transfer from M^{n+} cations to $[BH_4]^-$ anions is a key feature to determine the stability of $M(BH_4)_n$. Specifically, there exists a positive linear relationship between the formation enthalpy ΔH_{boro} of $M(BH_4)_n$ and the Pauling electronegativity χ_p of the cation, $\Delta H_{boro} = 248.7\chi_p - 390.8$ [5,6]. Moreover, the thermal desorption experiments of $M(BH_4)_n$ indicate that the hydrogen desorption temperature T_d has a negative correlation with χ_p [7]. For example, $LiBH_4$ needs to be heated to above 673 K to release most of the hydrogen due to the high enthalpy of 75 kJ/mol, which is unsuitable for practical applications in the automotive sector.

Presently, NH_3BH_3 (AB) has been regarded as a promising hydrogen storage media for on-board applications owing to its remarkable high hydrogen content (19.6 wt%) and satisfactory air stability. Unfavorably, the thermal dehydrogenation of AB is accompanied with the emission of toxic gases (e.g. NH_3, B_2H_6, $B_3H_6N_3$) which is harmful to fuel cell, and the kinetics of dehydrogenation of AB is also sluggish. To address above issues, substantial efforts have been made to optimize the dehydrogenation performance of AB. The effect of metal chloride additives and metal hydride additives on dehydrogenation performance of AB was studied systematically by Yuki Nakagawa *et al.* The results indicated that the halide with higher χ_p of cation and $MAlH_4$ (M = Na, Li) could not only decrease the onset temperature of hydrogen release but also effectively suppress the emission of toxic gases [8,9]. For the halide, M^{n+} in MCl_n can work as a Lewis acid site to initiate the AB dehydrocoupling reaction by inducing changes in the electronic state of N. In addition, nanoconfinement is another effective strategy to optimize the dehydrogenation performance of AB. For instance, Gutowska *et al.* reported nanoconfinement of AB in mesoporous silica could significantly decrease the dehydrogenation temperature [10]. Our group also performed the research on nanoconfinement to modify the thermodynamics and kinetics of AB and indicated that the pore size,

Peer review under responsibility of Chinese Materials Research Society.
* Corresponding authors.
E-mail addresses: y.jia@griffith.edu.au (Y. Jia), meouyang@scut.edu.cn (L. Ouyang).

https://doi.org/10.1016/j.pnsc.2018.02.002
Received 8 January 2018; Accepted 2 February 2018
Available online 15 March 2018

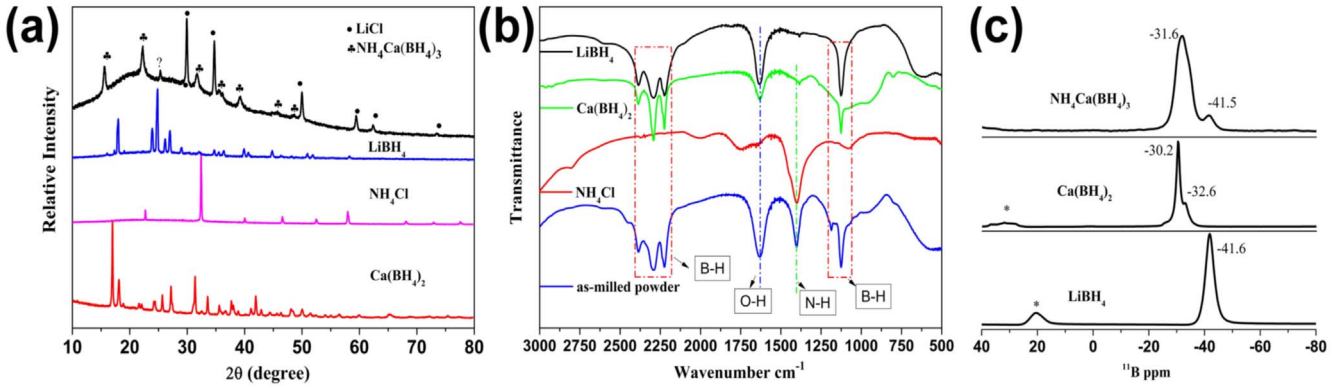

Fig. 1. (a) XRD patterns of starting materials and as-milled sample; (b) FTIR spectra of starting materials and as-milled sample; (c) ^{11}B NMR spectra of $LiBH_4$, $Ca(BH_4)_2$, and $NH_4Ca(BH_4)_3$. Side bands are indicated by * .

unsaturated bonds and metal ions are key to achieve this modification [11–13]. It is reported that the improved dehydrogenation performance of AB confined by a metal organic framework (MOF: JUC-32-Y), which lowers the onset temperature of nanoconfined system to only ~50 °C while the dehydrogenation of neat AB is at ~100 °C [11]. Furthermore, loading AB into low-density porous aromatic framework (PAF-1) can significantly improve the overall hydrogen gravimetric capacity due to the light C and H elements in PAF-1 host as compared to heavy MOF based scaffolds [9]. Lithium-catalyzed dehydrogenation of AB within mesoporous carbon framework (Li-CMK-3) is also a good tactics, and the dehydrogenation capacity of Li-CMK-3 nanoconfined AB system can reach to ~7 wt% at around 60 °C. Simultaneously, the undesirable volatile byproducts can be entirely suppressed due to the synergistic effects of nanoconfinement and Li catalysis [13].

Ammonium borohydride (NH_4BH_4), possessing the highest gravimetric hydrogen content (24.5%), is another promising candidate for hydrogen storage. NH_4BH_4 was firstly reported to be synthesized by a metathesis reaction between NH_4F and $NaBH_4$ in 1958 [14]. However, NH_4BH_4 is unstable above − 40 °C and will decompose at room temperature. Therefore, stabilization of NH_4BH_4 is an important prerequisite to realize its practical application. Recently, it is reported that solid NH_4BH_4 is stable for weeks at room temperature under a pressure of 0.5 GPa [15,16], whereas it is not a practical approach via such an extreme condition. Nielsen *et al.* tried to stabilize NH_4BH_4 by nanoconfinement in mesoporous silica but it was not achievable [15]. However, dual-cation borohydrides seem to be a feasible method to stabilize the borohydrides. Knight *et al.* successfully synthesized $KAl(BH_4)_4$ hypersalt, which could stabilize the volatile liquid aluminum borohydride into a manageable solid by combination with KBH_4, enhancing remarkably the thermal stability [17]. Using the same method, Schouwink *et al.* synthesized complex borohydride $NH_4Ca(BH_4)_3$ which is stable at room temperature [18,19], but the hydrogen release from this compound has not been systematically investigated.

In this work, a dual-cation perovskite-type borohydride, $NH_4Ca(BH_4)_3$, was fabricated via ball milling of $Ca(BH_4)_2$, $LiBH_4$ and NH_4Cl according to the literatures [18,19]. Due to the high theoretical hydrogen content of $NH_4Ca(BH_4)_3$, it is demanded to study its dehydrogenation property and dehydriding pathway. The initial dehydrogenation temperature of $NH_4Ca(BH_4)_3$ is relatively low (at about 65 °C), whereas the overall activation energy of decomposition is still about 226.1 kJ/mol, suggesting a stepwise dehydriding pathway of $NH_4Ca(BH_4)_3$. The further FTIR and NMR results reveal that the initial dehydrogenation is due to the destabilization of H^+ in NH_4 and H^- in BH_4 followed by the subsequent dehydrogenation steps arising from the decomposition of homologous NH_3BH_3 (the rest NH_3 from NH_4 and BH_3 from one BH_4) and $Ca(BH_4)_2$ at a high temperature, respectively.

2. Experimental section

$Ca(BH_4)_2$ (product NO. 695254) and $LiBH_4$ (95%) were used as purchased from Sigma-Aldrich. NH_4Cl was purchased from Tianjin Damao Chemical Reagent Factory. The starting materials were used as received without further purification. $NH_4Ca(BH_4)_3$ was synthesized in according with the reference [18]. $Ca(BH_4)_2$, $LiBH_4$ and NH_4Cl (1 g in total) were mixed and put into a stainless ball milling jar. The ball-to-powder mass ratio was set to 50:1 at the start. The mechanochemical reaction was then undertaken at 500 rpm for 2 h using a type of planetary ball mill (QM-3SP4, Nanjing, China) at room temperature. To prevent overheating, the milling process was performed every 2 min milling by breaking 5 min for 60 cycles. All sample handling was performed in an Ar-filled glovebox.

The ball milled product was analyzed by powder diffractometer (XRD, PANalytical X'PERT) using Cu Ka radiation (λ = 1.5406 Å). The qualitative analysis of FTIR using an iS50 Fourier transform infrared spectrometer was applied to the samples in our experiments. Differential scanning calorimetry (DSC) analysis was performed using a high-pressure differential scanning calorimetry (SETARAM, France). Temperature programmed desorption (TPD) measurement was conducted on an automatic Sieverts-type apparatus (AMC, HP2000). The isothermal dehydrogenation kinetic test was conducted initially under vacuum at differently specific temperature. About 230 mg sample was put into sample holder. ^{11}B solid-state NMR experiments were carried out at room temperature on a Bruker Advance 400 NMR spectrometer operating at 9.7 T. Scanning electron microscopy (SEM) was carried out on a Philips XL-30 FEG

3. Results and discussion

3.1. Synthesis of $NH_4Ca(BH_4)_3$

Synthesis of $NH_4Ca(BH_4)_3$ from $LiBH_4$, $Ca(BH)_2$ and NH_4Cl is based on a metathesis reaction as following Eq. (2):

$$LiBH_4 + Ca(BH_4)_2 + NH_4Cl \rightarrow NH_4Ca(BH_4)_3 + LiCl \quad (2)$$

The X-ray diffraction (XRD) characterization was applied to the starting materials and the as-milled sample. As shown in Fig. 1a, the peaks of NH_4Cl, $LiBH_4$ and $Ca(BH_4)_2$ have completely disappeared and new peaks appeared after ball-milling the starting materials for 2 h. The new XRD peaks shown in Fig. 1b are assigned to $NH_4Ca(BH_4)_3$ and by-product LiCl respectively, which is in agreement with the reported data [19]. In addition, a broad peak centered at approximately 20 degree is attributed to the tape used to protect the sample from being exposed to air.

Accordingly, the FTIR patterns in Fig. 1b are also applied to reveal the milled sample. The FTIR spectra of NH_4 in NH_4Cl have characteristic band at 1402 cm^{-1} that also appears in the FTIR spectra of the as-milled sample. Additionally, the infrared characteristic peak of -BH_4 (stretching vibration: 2200 cm^{-1}~2400 cm^{-1}, and deformation vibration: 1128 cm^{-1}) was also detected by FTIR in the as-milled sample; that is to say, the newly formed composite coexists with -BH_4 and -NH_4, and no reaction occurred between -NH_4 and -BH_4 during ball milling.

To specify the difference between $LiBH_4$, $Ca(BH_4)_2$ and $NH_4Ca(BH_4)_3$, ^{11}B NMR were carried out and the results were given in Fig. 1c. The chemical shift of $LiBH_4$ observed in the ^{11}B NMR spectrum was − 41.6 ppm. There are two peaks appeared in the spectra of $Ca(BH_4)_2$ which can be assigned to α-$Ca(BH_4)_2$ (− 30.2 ppm) and β-$Ca(BH_4)_2$ (− 32.6 ppm), respectively. Notably, The chemical shift of $NH_4Ca(BH_4)_3$ observed in the ^{11}B NMR spectrum is significantly different from $LiBH_4$ and $Ca(BH_4)_2$, centered at − 31.6 ppm. Additionally, a small signal is also observed at − 41.5 ppm, indicating a trace amount of unreacted $LiBH_4$ in the as-milled sample. All the above characterization confirms the formation of $NH_4Ca(BH_4)_3$ by ball milling.

3.2. Thermal decomposition performance of $NH_4Ca(BH_4)_3$

The complex borohydride $NH_4Ca(BH_4)_3$ has a high gravimetric hydrogen density of 15.7 wt%. However, the proper thermodynamic stability of $NH_4Ca(BH_4)_3$ is the prerequisite for considering its application in the on-board hydrogen storage. Therefore, the thermal decomposition and temperature programmed desorption (TPD) of $NH_4Ca(BH_4)_3$ were performed using DSC and automatic Sieverts-type apparatus at a heating rate of 2 K/min. The results are shown in Fig. 2a. It should be mentioned that the as-milled powders were directly used for testing without removal of the by-product LiCl (the same in the following tests). According to the TPD curve in the Fig. 2a, $NH_4Ca(BH_4)_3$ experienced a multistep decomposition during heating process. It can be seen that the $NH_4Ca(BH_4)_3$ initially releases a minor amount (~0.9 wt%) of hydrogen before 100 °C. Subsequently, there is about 3.1 wt% hydrogen released from the second step (P2) with an onset temperature of 110 °C. Afterwards in P3, only a trace amount (~0.7 wt %) of hydrogen was produced from 210 to 260 °C. Finally in P4, much more hydrogen (4.6 wt%) was desorbed with elevating temperature to 420 °C. Briefly, the $NH_4Ca(BH_4)_3$ can release about 9.3 wt% hydrogen throughout the heating process. As compared to TPD results of individual $LiBH_4$ [20,21] (10.5 wt% hydrogen released at 600 °C) and $Ca(BH_4)_2$ [22] (8.1 wt% hydrogen released at 480 °C), $NH_4Ca(BH_4)_3$ can lease the majority of hydrogen at lower temperatures. DSC curve in Fig. 2a also indicated a stepwise decomposition. Combined with the TPD profile, the first endothermic peak at below 100 °C corresponded to the first decomposition of $NH_4Ca(BH_4)_3$ (P1 stage), indicating the initial hydrogen release from $NH_4Ca(BH_4)_3$. After that, there were two endothermic peaks at 93 and 118 °C appear without hydrogen evolution as shown in the TPD curve, which will be discussed later. Subsequently, a broad DSC exothermic peak was observed after the third endothermic peak, ranging from 120 to 145 °C, which was corresponding to the second dehydrogenation P2 in TPD curve (3.1 wt% weight loss). The broad exothermic peak (120 ~ 145 °C) and the third exothermic peak (~118 °C) are similar to the DSC measurement results reported for AB [23–25]. An endothermic peak at 225 °C corresponded to P3 stage accompanied with about 0.7 wt% hydrogen desorption. Additionally, there were two endothermic peaks corresponding to the P4 stage (~ 4.6 wt% hydrogen release) appearing at temperatures of 340 °C and 352 °C, which are in agreement with the DSC measurement results for a mixed borohydride of $LiBH_4$ and $Ca(BH_4)_2$ [26]. In reference [26], it is reported that the addition of a certain amount of $LiBH_4$ in $Ca(BH_4)_2$ can reduce the dehydrogenation temperature of the $LiBH_4$-$Ca(BH_4)_2$ composite to 370 °C. It is reported that the first decomposition peak temperatures of $LiBH_4$ [27] and $Ca(BH_4)_2$ [28] by DSC are at about 425 °C and 360 °C respectively, which are significantly higher than that of $NH_4Ca(BH_4)_3$ (84 °C). Specifically, the DSC curve of $LiBH_4$ shows two sharp endothermic peaks which correspond to the structural transition (116 °C) and the phase melt (286 °C), followed by two broad endothermic peaks corresponding to thermal dehydrogenation at around 425 and 550 °C [27]. For $Ca(BH_4)_2$, two endothermic peaks can be observed at about 360 and 440 °C in the DSC curve, indicating two steps

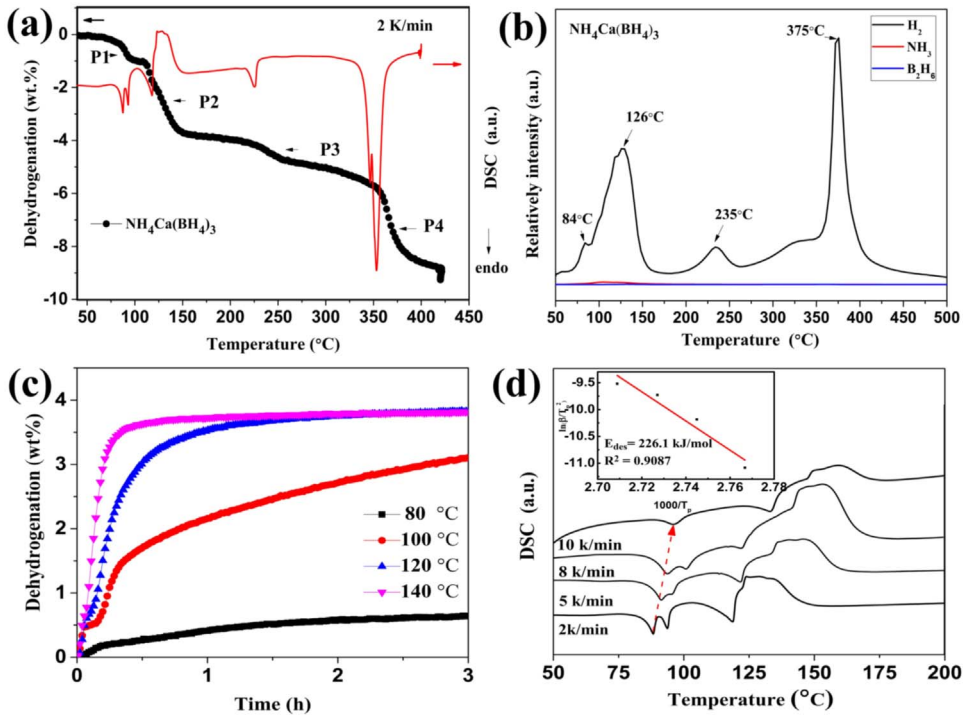

Fig. 2. (a) TPD curve and DSC curve of $NH_4Ca(BH_4)_3$; (b) MS profiles of $NH_4Ca(BH_4)_3$; (c) isothermal hydrogen desorption curves of $NH_4Ca(BH_4)_3$ at varied temperatures; (d) DSC curves of $NH_4Ca(BH_4)_3$ using varied heating rates and the inset shows the Kissinger plot of thermal desorption curves at a heating rate between 2 K/min and 10 K/min.

of desorption [28].

The $NH_4Ca(BH_4)_3$ decomposition behavior was also investigated using TPD-MS at a heating rate of 5 K/min. Distinctly, multiple hydrogen desorption peaks were shown in Fig. 2b. The first dehydrogenation peak occurred at a low temperature (~84 °C) with the release of pure hydrogen, which is superior to $LiBH_4$ [20] and $Ca(BH_4)_2$ [22]. At a higher temperature, a broad dehydrogenation peak, which means a large amount of hydrogen, was released at a wide temperature range (90–160 °C). Another sharp dehydrogenation peak was observed at 375 °C, suggesting the rest hydrogen has been almost released at this step, which is coincided with the TPD results. Notably, there is almost no diborane (B_2H_6) and NH_3 released throughout the whole thermal decomposition of $NH_4Ca(BH_4)_3$. Compared to NH_3BH_3 [12], the result of TPD-MS in Fig. 2b illustrated that the perovskite-type $NH_4Ca(BH_4)_3$ constructed from NH_4BH_4 and $Ca(BH_4)_2$ can effectively inhibit the release of the impurity gas and exhibit a multi-step decomposition.

As $NH_4Ca(BH_4)_3$ possesses high dehydrogenation capacity and low dehydrogenation temperature, isothermal experiments have been carried out at temperatures of 80, 100, 120 and 140 °C, respectively. The results were given in Fig. 2c. At 80 °C, the dehydrogenation kinetics of $NH_4Ca(BH_4)_3$ was extremely sluggish and the desorbed amount of hydrogen was about 0.6 wt% in 3 h. The released hydrogen at this temperature can be attributed to the first step of dehydrogenation of $NH_4Ca(BH_4)_3$ supported by TPD results. With the increase of isothermal temperature, the amount of hydrogen and the dehydrogenation kinetics of $NH_4Ca(BH_4)_3$ were both significantly enhanced. It can be observed that 3.1 wt% hydrogen was released in 3 h at a temperature of 100 °C, which is ascribed to the dehydrogenation stage of P2 as shown in Fig. 2a. The higher temperature enables the hydrogen release in a fast kinetics, e.g. release 3.8 wt% (~5.4 wt% if the hydrogen is estimated from the mass of $NH_4Ca(BH_4)_3$ rather than the whole composite) hydrogen in 2 h and 25 min at 120 and 140 °C, respectively. This suggests that the $NH_4Ca(BH_4)_3$ experiences the same dehydrogenation process during heating at these two temperatures.

To further understand the dehydrogenation kinetics mechanism of $NH_4Ca(BH_4)_3$, we measured the DSC profiles at different heating rates, from 2 K/min to 10 K/min, and estimated the activation energy for the desorption process (Fig. 2d) by using Kissinger Eq. (3)[29]

$$d[ln(\beta/T_p^2)]/d(1/T_p) = -E_a/R \quad (3)$$

where β is the heating rate, T_p is the peak temperature, E_a is the activation energy and R is the gas constant. Though multiple peaks on each curve, the first endothermic peak is believed to be related to the initial decomposition of $NH_4Ca(BH_4)_3$, which could be evidenced by the TPD and DSC results. The Kissinger plots, $\ln(\beta/T_p^2)$ as a functional of the inverse of $1000/T_p$ is shown in the inset of Fig. 2d. From the slope of the fit line, the E_a was estimated to be 226.1 kJ/mol ($R^2 = 0.91$).

3.3. Decomposition pathway of $NH_4Ca(BH_4)_3$

The above results indicate that the $NH_4Ca(BH_4)_3$ experiences a multi-step decomposition process during heating. To get in-depth insight into desorption process of $NH_4Ca(BH_4)_3$, four samples were treated at differently specified temperatures of 85, 150, 240 and 400 °C, respectively. When the dehydrogenation process reached equilibrium at a specified temperature, the products after dehydrogenation were collected and tested by FTIR. The FTIR spectra were shown in Fig. 3. For comparison purpose, the FTIR spectrum of NH_3BH_3 was also given, in which the standard peaks clearly indicates the BH_3 and NH_3, e.g. the B-H stretching vibration (1068 cm^{-1}, 1164 cm^{-1}) and the B-H deformation vibration (2343 cm^{-1}) for BH_3 and 1067, 1388 and 3317 cm^{-1} for NH_3. The FTIR confirms $NH_4Ca(BH_4)_3$ in Fig. 3b, e.g. stretching vibration: 2200 cm^{-1}~2400 cm^{-1} and deformation vibration: 1128 cm^{-1}) for BH_4. When $NH_4Ca(BH_4)_3$ treated at 85 °C, both the peaks of BH_4 and BH_3 co-existed in the FTIR as seen in Fig. 3c. However, the intensity of infrared characteristic peaks at 3317 and 1388 cm^{-1} was obviously weakened. Fig. 3c showed that a reaction between BH_4 and NH_4 was occurred at 85 °C and an equivalent of hydrogen was released; that is to say, a reaction took place at 85 °C as shown in formula (4).

$$NH_4^+ + BH_4^- \rightarrow NH_3BH_3 + H_2 \quad (4)$$

When the temperature rose to 150 °C, as shown in Fig. 3d, only the characteristic peaks of BH_4 were detected whereas the characteristic peaks of BH_3 disappeared completely. It is remarkable that the peak of N-H at 1388 cm^{-1} further disappeared with the increase of temperature to 240 °C (Fig. 3e), suggesting the multi-step dehydrogenation process of homologous NH_3BH_3 [19]. According to the Fig. 3f, the characteristic infrared peaks of B-H disappeared completely, which means the decomposition of borohydride happened when treated at 400 °C.

For further understanding of the dehydrogenating mechanism of $NH_4Ca(BH_4)_3$, the solid state ^{11}B NMR spectroscopy was also applied to further analyze the dehydrogenation pathways of $NH_4Ca(BH_4)_3$. As shown in Fig. 4, seven samples treated at different temperatures were tested by NMR. Apparently, in ^{11}B NMR spectrum, a sharp peak at a chemical shift of − 31.6 ppm was observed which can be assigned to -BH_4 in $NH_4Ca(BH_4)_3$. The resonance at − 31.6 ppm disappeared completely in the sample treated at 85 °C, while other three different chemical shifts appeared at − 30.1, − 34.1 and − 41.3 ppm. The chemical shifts at − 30.1 ppm, − 34.1 ppm and − 41.3 ppm can be assigned to NH_3BH_3 [30], β-$Ca(BH_4)_2$ [31,32] and $LiBH_4$ [33,34], respectively. Evidenced by the formation of $LiBH_4$ at 85 °C in NMR (Fig. 4) and the second endothermic peak at 93 °C without the emission of hydrogen in DSC curves (Fig. 2a), it is suggested that -BH_4 in $Ca(BH_4)_2$ was partially substituted by Cl^- in LiCl after the first decomposition of $NH_4Ca(BH_4)_3$ [35,36]. The intercalation of Cl^- in Li/Ca based borohydride is reported to enable the deformation of lattice structure, leading to destabilization of the B-H bonding [29]. To the sample treated at 95 °C, the experimental NMR curve in Fig. 4 reflects the disappearance of the chemical shifts at − 30.1 ppm accompanied by the appearance of three differently new signals centered at around 1, 11 and 23 ppm that are assigned to the boron nitride compounds,-BN_4, B(-$NBH)_2$(-NB_2) and BH(-$NBH)_2$ [37]. However, the signals of β-$Ca(BH_4)_2$ (− 34.1) and $LiBH_4$ (− 41.3 ppm) remain in Fig. 4, indicating their decomposition temperature are higher than 95 °C. Compared with the sample treated at 85 °C, the increased temperature only leads to the decomposition of NH_3BH_3. In the samples treated at 95 °C and 150 °C, the ^{11}B NMR signals do not change obviously, indicating a same reaction between -NH_4 and -BH_4 in $NH_4Ca(BH_4)_3$. However, the chemical shift at 1 ppm nearly disappeared while the intensity of the signal at 23 ppm significantly enhanced. This suggests that the boron nitride compounds further decomposed at higher temperature. For samples dehydrogenated at 400 °C, all the signals of -BH_4 disappeared, leaving a broad NMR peak which could be assigned to CaB_6 (14.6 ppm) and B (− 1 ppm) [31,32] in Fig. 4. These results indicate that the borohydrides were decomposed when treated at 400 °C.

In short, the decomposition of $NH_4Ca(BH_4)_3$ can be considered as the combinative decomposition of NH_4BH_4 and $Ca(BH_4)_2$ at different temperatures. At a temperature of 84 °C, one equivalent hydrogen molecule is desorbed firstly by the combination of H^+ in -NH_4 and H^- in -BH_4 (equation 5), corresponding to the first endothermic peak in DSC curve and 0.9 wt% weight loss in TPD curve (Fig. 2a). Subsequently, due to the presence of by-product LiCl, an ion substitution reaction occurs between LiCl and $Ca(BH_4)_2$ in the heating process (equation 6), which is consistent with the second endothermic peak at 93 °C in DSC curve and no weight loss is observed in TPD curve. With the temperature elevating, the dehydrogenation of structural hydrogen in homologous NH_3BH_3 is initiated and its exothermic peak at ~132 °C is observed in DSC curve accompanying with 3.8 wt% hydrogen desorption in TPD curve (equation 7). When the temperature is further increased to

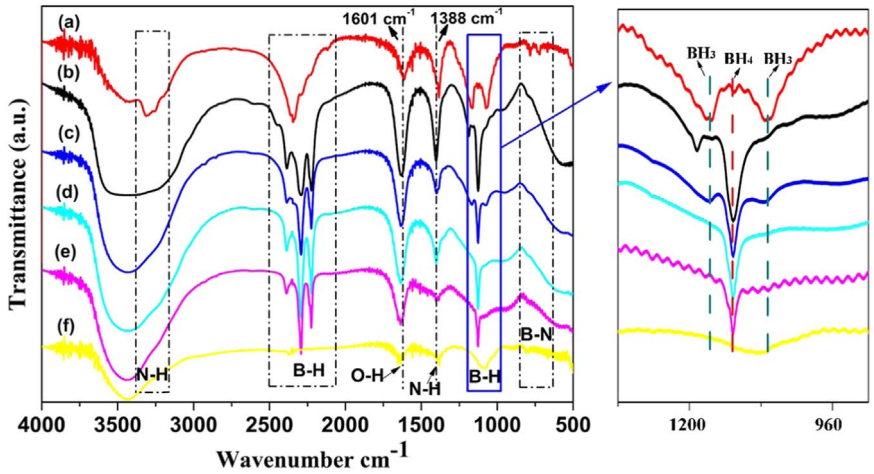

Fig. 3. FTIR spectra of NH_3BH_3 (a), as-milled $NH_4Ca(BH_4)_3$ (b) and $NH_4Ca(BH_4)_3$ samples heated at different temperature: 85 °C (c); 150 °C (d); 240 °C (e); 400 °C (f).

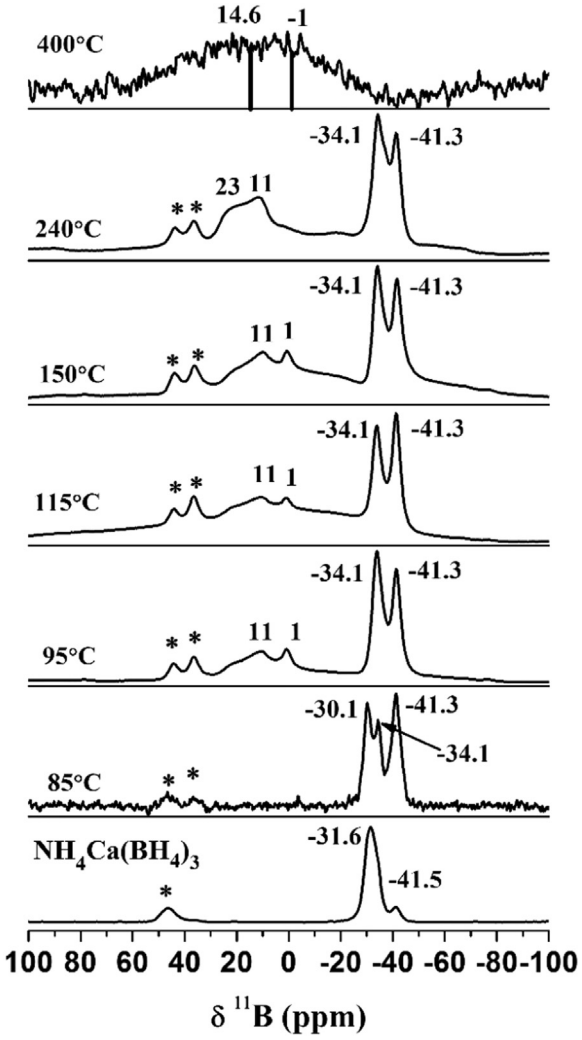

Fig. 4. ^{11}B NMR of $NH_4Ca(BH_4)_3$ heated to varied temperature. Side bands are indicates by *.

above 400 °C, such a high temperature enables the thermal decomposition of metal borohydrides ($Ca(BH_4)_2$ in equation 8 and $LiBH_4$ in equation 9), desorbing the rest hydrogen (P4 stage in TPD curve with 4.6 wt% hydrogen release) which is consistent with the last two endothermic peaks at 340 °C and 352 °C in DSC curve, respectively. The whole process is summarized as follows:

$$NH_4Ca(BH_4)_3 \rightarrow Ca(BH_4)_2NH_3BH_3 + H_2 \quad (5)$$

$$Ca(BH_4)_2 + LiCl \rightarrow Ca(BH_4)_xCl_{2-x} + Li(BH_4)_yCl_{1-y} \quad (6)$$

$$NH_3BH_3 \rightarrow x\ [-BN_4 + B(-NBH)_2(-NB_2) + BH(-NBH)_2]_{mixture} + y\ H_2 \quad (7)$$

$$Ca(BH_4)_2 \rightarrow 2/3\ CaH_2 + 1/3\ CaB_6 + 10/3H_2 \quad (8)$$

$$LiBH_4 \rightarrow LiH + B + 3/2H_2 \quad (9)$$

4. Conclusion

In summary, fabricating dual-cation borohydride is demonstrated as an effective strategy to tailor the hydrogen storage performance of NH_4BH_4, which can not only stabilize NH_4BH_4 at room temperature but also inhibit the evolution of impurity gas. The onset temperature of as-prepared $NH_4Ca(BH_4)_3$ is relatively low, at around 65 °C. Notably, about 3.8 wt% (~5.4 wt% if the hydrogen is estimated from the mass of $NH_4Ca(BH_4)_3$ rather than the whole composite) hydrogen can be released at 140 °C within only 25 min. Furthermore, the dehydrogenation kinetics is analyzed by using Kissinger's method and the activation energy of decomposition is calculated about 226.1kJ/mol. Characterization results on dehydrogenation process of $NH_4Ca(BH_4)_3$ by FTIR and NMR indicate that the initial dehydrogenation is due to the destabilization of H^+ in NH_4 and H^- in BH_4 followed by the subsequent dehydrogenation steps arising from the decomposition of homologous NH_3BH_3 and $Ca(BH_4)_2$, respectively.

Acknowledgment

This work was supported by the Foundation for Innovative Research Groups of the National Natural Science Foundation of China (No. NSFC51621001), National Natural Science Foundation of China Projects (Nos. 51431001 and 51771075) and by International Science & Technology Cooperation Program of China (2015DFA51750). Yi Jia thanks the financial support from Australia Research Council Discovery Early Career Researcher Award (ARC DE180101030). The Project Supported by Guangdong Province Universities and Colleges Pearl River Scholar Funded Scheme (2014) is also acknowledged.

References

[1] S. Orimo, et al., J. Alloy. Compd. 404–406 (2005) 427–430.
[2] G. Xia, et al., Adv. Sci. 4 (9) (2017).
[3] G. Xia, et al., J. Mater. Chem. A 1 (5) (2013) 1810–1820.
[4] G. Xia, et al., Acta Mater. 61 (18) (2013) 6882–6893.
[5] Y. Nakamori, et al., Phys. Rev. B 74 (4) (2006).

[6] P. Vajeeston, et al., J. Alloy. Compd. 387 (1–2) (2005) 97–104.
[7] Y. Nakamori, et al., J. Alloy. Compd. 446–447 (2007) 296–300.
[8] Y. Nakagawa, et al., J. Mater. Chem. A 2 (11) (2014) 3926.
[9] Y. Nakagawa, et al., J. Chem. Eng. Data 61 (5) (2016) 1924–1929.
[10] A. Gutowska, et al., Angew. Chem. Int. Ed. 44 (23) (2005) 3578–3582.
[11] Z. Li, et al., J. Am. Chem. Soc. 132 (5) (2010) 1490–1491.
[12] Y. Peng, et al., J. Phys. Chem. C 116 (49) (2012) 25694–25700.
[13] L. Li, et al., Adv. Funct. Mater. 19 (2) (2009) 265–271.
[14] R. Parry, D. Schultz, P. Girardot, J. Am. Chem. Soc. 80 (1) (1958) 1–3.
[15] T.K. Nielsen, et al., Dalton Trans. 42 (3) (2013) 680–687.
[16] R. Flacau, et al., Chem. Commun. 46 (48) (2010) 9164–9166.
[17] D.A. Knight, et al., J. Phys. Chem. C. 117 (39) (2013) 19905–19915.
[18] P. Schouwink, et al., Nat. Commun. 5 (2014).
[19] P. Schouwink, et al., Energies 8 (8) (2015) 8286–8299.
[20] B.J. Zhang, B.H. Liu, Int. J. Hydrog. Energy 35 (14) (2010) 7288–7294.
[21] L. Guo, et al., Int. J. Hydrog. Energy 38 (1) (2013) 162–168.
[22] H. Chu, et al., Dalton Trans. 39 (44) (2010) 10585–10587.
[23] F. Baitalow, et al., Thermochim. Acta 391 (1) (2002) 159–168.
[24] T. He, et al., Chem. Mater. 21 (11) (2009) 2315–2318.
[25] R. Benzouaa, et al., Thermochim. Acta 509 (1–2) (2010) 81–86.
[26] J.Y. Lee, et al., J. Phys. Chem. C. 113 (33) (2009) 15080–15086.
[27] S. Cahen, et al., J. Power Sources 189 (2) (2009) 902–908.
[28] J. Mao, et al., J. Alloy. Compd. 500 (2) (2010) 200–205.
[29] H.E. Kissinger, Anal. Chem. 29 (11) (1957) 1702–1706.
[30] A.C. Stowe, et al., Phys. Chem. Chem. Phys. 9 (15) (2007) 1831–1836.
[31] C. Bonatto Minella, et al., J. Phys. Chem. C 115 (5) (2011) 2497–2504.
[32] Y. Kim, et al., J. Phys. Chem. C 116 (6) (2012) 4330–4334.
[33] O. Friedrichs, et al., Chem. Mater. 22 (10) (2010) 3265–3268.
[34] L. Mosegaard, et al., J. Alloy. Compd. 446–447 (2007) 301–305.
[35] C. Rongeat, et al., Int. J. Hydrog. Energy 36 (1) (2011) 247–253.
[36] J.Y. Lee, et al., J. Alloy. Compd. 506 (2) (2010) 721–727.
[37] T. Kobayashi, et al., J. Phys. Chem. C 118 (34) (2014) 19548–19555.